

pubs.acs.org/JPCC Article

Metal—Organic Framework as a Dual Support for Organic Photosensitizers and Single-Atom Catalysts

Humphrey Chiromo, James Nyakuchena, Daniel Streater, Qiushi Ma, Christopher Turchiano, Xiaoyi Zhang, Jing Gu, and Jier Huang*



Cite This: J. Phys. Chem. C 2023, 127, 20354-20359



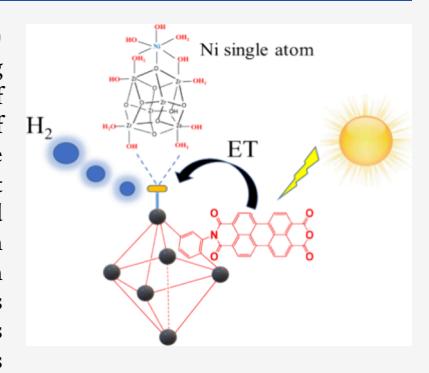
ACCESS

III Metrics & More

Article Recommendations

s Supporting Information

ABSTRACT: Metal—organic framework (MOF)-supported single-atom catalysts (SACs) possess integrated unique capabilities of both MOF and SACs, which represent a promising class of catalysts for photocatalytic applications. Herein, we report the incorporation of nickel (Ni) SACs onto its zirconium node and the functionalization of the organic linker of the zirconium MOF with perylene tetracarboxylic dianhydride (PDA), resulting in the formation of a hybrid MOF (denoted as Ni-PiU) with significantly enhanced light absorption ability in the visible region. Using the combination of time-resolved emission and X-ray absorption spectroscopy, we show that efficient charge separation occurs by electron transfer from incorporated PDA to Ni SACs with super slow charge recombination dynamics. As a result of these important photophysical properties, Ni-PiU MOF exhibits excellent photocatalytic activity and durability for the hydrogen evolution reaction. This work demonstrates the unique ability of MOFs as a dual platform to incorporate both SACs



and a light absorption unit into their framework, providing a promising strategy for rational design of next-generation photocatalytic materials.

1. INTRODUCTION

Reducing the size of metal nanoparticle catalysts to form single-atom catalysts (SACs) has emerged as one of the best ways to enhance the catalysts' activity and selectivity^{1,2} due to their unique characteristics, such as nearly 100% atom utilization and well-defined active sites.³⁻⁶ These attributes position them as a crucial link between homogeneous and heterogeneous catalysts.^{7,8} However, the broad application of SACs in catalytic reactions faces challenges due to their poor stability as they possess high surface energy, leading to their tendency to aggregate and form nanoclusters or nanoparticles. 9-12 To overcome this challenge, various supports with high surface area and binding sites, such as metal oxides, carbon-based materials, and porous materials, have been employed to anchor SACs. Among them, metal—organic frameworks (MOFs), a class of porous crystalline materials comprised of metal clusters and organic linkers, represent one of the most promising platforms for immobilizing SACs. 15-17 It has been shown that immobilizing SACs on MOFs can integrate the unique properties of both SACs and MOFs, leading to their remarkable catalytic activity, selectivity, and stability toward various catalytic reactions. 18-20 In the realm of photocatalysis, where MOF-supported SACs often find application, MOFs often function as photosensitive units.^{21,22} However, MOFs typically possess a large band gap, which results in poor visible light-harvesting properties.²³ Owing to their structural versatility, MOFs can be modified by functionalizing their building blocks to incorporate a lightabsorbing unit²⁴ or encapsulating semiconductor/dye molecules.^{23,25} This alteration allows the adjustment of their band gap and enhances their visible light absorption ability.^{26,27}

In this work, we report the immobilization of Ni SACs on the zirconium cluster of UiO-66-NH₂ MOF and the postsynthetic modification of its linker with 3,4,9,10-perylene tetracarboxylic dianhydride (PDA), an organic molecule with a broad absorption edge in the visible region. ²⁸ We show that the functionalization of the MOF linker with PDA significantly enhances the light-harvesting property of UiO-66-NH₂ MOF by extending its absorption to the visible region. Using a combination of time-correlated single-photon counting (TCSPC) and X-ray transient absorption (XTA) spectroscopy, we demonstrate that efficient charge separation occurs via electron transfer from incorporated PDA to Ni SACs following the excitation of PDA. As a result of these exceptional photophysical properties, the system becomes an effective photocatalyst for hydrogen evolution reaction (HER).

Received: July 25, 2023 Revised: August 29, 2023 Published: October 9, 2023





Scheme 1. Synthetic Route of Ni-PiU

(i) A solution containing zirconium chloride, 2-amino terephthalic acid, dimethylformamide, and acetic acid was heated for 24 h, which leads to the formation of UiO-66-NH₂; (ii) a mixture of imidazole, as-synthesized UiO-66-NH₂, and PDA was refluxed under a nitrogen atmosphere for 12 h, resulting in the formation of PiU; (iii) a dispersion containing the as-synthesized PiU, nickel chloride hexahydrate, and dimethylformamide was heated at 85°C for 2 h, which leads to the final product Ni-PiU.

2. EXPERIMENTAL METHODS

- **2.1. Materials and Chemicals.** Zirconium(IV) chloride (99.5% Zr Strem Chemicals), nickel(II) chloride hexahydrate (Sigma-Aldrich), 3,4,9,10-perylenetetracarboxylic dianhydride (PDA 95% AmBeed), imidazole (99% Alfa Aesar), and 2-amino-terephthalic acid (99% Acros Organics) were used without further purification.
- **2.2. Synthesis of UiO-66-NH₂.** Synthesis of UiO-66-NH₂ was based on the previously reported procedure for UiO-66-type MOF with slight modification.²⁹ Briefly, 233 mg (1 mmol) of zirconium(IV) chloride (ZrCl₄) and 181 mg (1 mmol) of 2-amino terephthalic acid (H₂ATA) were dissolved in 50 mL of dimethylformamide (DMF) solution containing 2 mL of acetic acid. The mixture was sonicated for 15 min and then transferred into a 100 mL glass tube. The flask was kept at 120 °C for 24 h. After cooling down the solution to room temperature, the resultant suspension was washed 3 times with ethanol and acetone and dried at 90 °C for 12 h in a vacuum dryer.
- **2.3.** Synthesis of PiU. UiO-66-NH₂ MOF modified with PDA (denoted PiU) was synthesized via the solvothermal method by reacting the synthesized UiO-66-NH₂ with PDA following the reported synthetic procedure for the PiU MOF.³⁰ Briefly, 600 mg of UiO-66-NH₂, 42 mg of PDA, and 10 g of imidazole were thoroughly mixed in a 100 mL round-bottom flask. The mixture was heated at 120 °C for 24 h under a nitrogen atmosphere. After cooling to room temperature, the red solution was dispersed in 250 mL of 2 M HCl and stirred vigorously for 12 h at room temperature. Excess PDA was removed by Soxhlet extraction with ethanol. The resultant solid was washed with ethanol (EtOH) and water (H₂O) and dried at 110 °C for 12 h.
- **2.4. Synthesis of Ni-PiU.** Forty milligram portion of PiU MOFs and 200 mg of nickel chloride hexahydrate (NiCl $_2$ ·6H $_2$ O) were dispersed in 6 mL of DMF in a glass vial. The mixture was heated at 85 °C for 2 h with continuous stirring. After cooling to room temperature, the solution was washed with ethanol and dried at 90 °C in a vacuum dryer.
- **2.5. Photocatalytic Hydrogen Evolution Reaction** (HER). Sample solution was prepared by dispersing 2.5 mg of the photocatalyst in a mixture of 4 mL of DMF, 1 mL of

triethylamine (TEA), and 100 μ L of deionized water in an 11 mL glass vial. Before irradiation with a xenon lamp of 300 W power, the solution was purged with nitrogen for 15 min. The hydrogen (H₂) evolved was quantitatively measured by taking 200 μ L of the gas sample from the glass vial headspace and injecting it into an Agilent 490 microgas chromatography system at different time duration after the initiation of the reaction.

- **2.6. Standard Characterization.** Powder X-ray diffraction patterns were obtained by utilizing a Rigaku MiniFlex (II) diffractometer with a Cu K α radiation source. The UV–visible absorption and diffuse reflectance spectra were collected by a Cary 5000 UV–vis–NIR spectrophotometer. FTIR measurements were conducted on solid samples with a Thermo Fisher Scientific Nicolet iS5 FTIR spectrometer equipped with an iD3 ATR accessory. Fluorescence and time-correlated single-photon counting (TCSPC) data were obtained by PTI fluorescence master systems. XPS measurements were performed by X-ray photoelectron spectroscopy (PHI 5600). The quantity of H_2 generated was determined by an Agilent 490 microgas chromatography system.
- **2.7. Steady-State X-ray Absorption (XAS) Spectroscopy.** XAS spectra were collected at beamline 12-BM-B, Advanced Photon Source, Argonne National Laboratory. The XAS results at the Ni K edge were obtained by using the fluorescence mode with a 13-element germanium detector with the Ni metal foil as the reference.
- 2.8. X-ray Transient Absorption (XTA) Spectroscopy. XTA spectra were taken at 11-ID-D beamline, Advanced Photon Source, Argonne National Laboratory, following our previously reported procedure. Briefly, the sample was prepared by dispersing 20 mg of Ni-PiU MOF in 70 mL of acetonitrile (MeCN), followed by sonication for 30 min. Optical pump pulses were generated by a regeneratively amplified Ti:sapphire laser (3 kHz, 100 fs (fwhm), 3 mJ). An 800 nm pulse was produced by a legend elite duo amplifier system implanted on a Micra-5 oscillator. The BBO crystal doubled the 800 nm signal, producing a 400 nm laser pulse. The X-ray probe and laser pump overlapped on a flowing sample with a 550 μ m diameter. The laser-on and laser-off spectra were obtained at different specified delay times after the laser pump pulse excitation of Ni-PiU. The difference

spectra were obtained by taking the difference between the laser-on and laser-off spectra.

3. RESULTS AND DISCUSSION

UiO-66-NH₂ was synthesized by a solvothermal reaction of ZrCl₄ with a 2-amino terephthalic acid ligand as illustrated in Scheme 1 (step (i)). Functionalization of the amino group of UiO-66-NH₂ with PDA was done through the imidization reaction (step (ii)), resulting in the formation of the C–N bond, which connects PDA to UiO-66-NH₂ MOF and forms PiU. Ni ions were immobilized on the Zr-oxo node by reacting the as-synthesized PiU with NiCl₂·6H₂O in a DMF solvent at 85 °C.

As shown in Figure 1a, the powder X-ray diffraction (XRD) patterns of UiO-66-NH₂, PiU, and Ni-PiU MOFs show similar

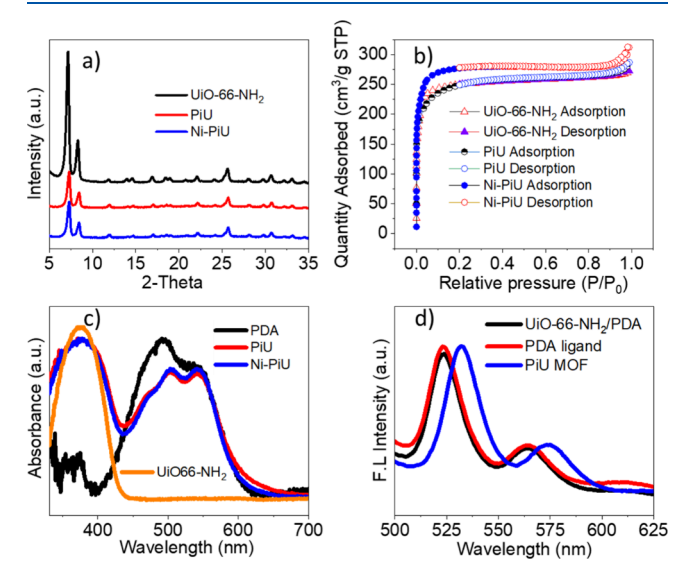


Figure 1. (a) Powder X-ray diffraction of UiO-66-NH₂, PiU, and Ni-PiU MOF; (b) BET isotherm of UiO-66-NH₂, PiU, and Ni-PiU; (c) diffuse reflectance UV—visible spectra of UiO-66-NH₂, PiU, Ni-PiU, and PDA ligand; (d) fluorescence emission spectra of UiO-66-NH₂/PDA (physical mixture of UiO-66-NH₂ with PDA), PDA, and PiU.

patterns as that of the reported UiO-66-NH₂ MOF,³² suggesting that PiU and Ni-PiU MOFs retained the crystallinity structure of the parent UiO-66-NH2 MOF upon the incorporation of PDA and Ni to UiO-66-NH2. This is further supported by the SEM images (Figure S1), which show that the postmodification of the parent MOF to form PiU and Ni-PiU does not affect the morphology of the MOFs. The specific surface area of the MOFs was analyzed by nitrogen sorption at 77 K. All three MOFs exhibited type I isotherms with surface areas of 820, 812, and 913 m^2/g for UiO-66-NH₂, PiU, and Ni-PiU (Figure 1b), respectively. The pore size distribution of all three MOFs falls in the range between 0.6 and 1.5 nm (Figure S2), confirming the microporous structure of these MOFs. The immobilization of PDA on UiO-66-NH2 is supported by the emergence of the asymmetric C=O stretching at 1690 cm⁻¹ as shown in the Fourier transform infrared (FTIR) spectrum (Figure S3), which can be attributed to the formation of an imide ring in PiU.³³ In addition, the absorption bands from 450 to 600 nm in the solid-state diffuse reflectance UV-visible spectra of PiU and Ni-PiU resemble the multiple monomeric π to π^* electronic transitions of PDA molecules (Figure 1c), 34 which confirms the incorporation of PDA to UiO-66-NH2 MOF and the enhancement of lightharvesting properties of the MOFs. This agrees with the observed color change from light yellow to red after PDA modification (Figure S4). The similarity of PiU to Ni-PiU absorption spectra suggests that modification of PiU with Ni²⁺ ions does not alter the light absorption properties of the MOFs. The emission spectra of PDA and a physical mixture of UiO-66-NH₂ and PDA (UiO-66-NH₂/PDA) exhibited similar spectral patterns (Figure 1d). In contrast, the emission spectrum of PiU showed a redshift with respect to that of both PDA and UiO-66-NH₂/PDA, which can be attributed to the electron-donating character of the amino (NH₂) group of the MOF, 35 and the extension of the π -system at the bay position of the PDA molecule.³⁶ This supports the successful functionalization of the organic linker in the UiO-66-NH₂ MOF with PDA, which is distinct from the presence of unbound PDA molecules.

Elemental composition of Ni-PiU examined by energy dispersive X-ray spectroscopy (EDX) confirms the existence of Zr, O, Cl, and Ni ions in Ni-PiU (Figure S5). In addition, the Ni content in Ni-PiU was found to be 2.8% wt Ni (Table S1) by inductively coupled plasma atomic emission spectroscopy (ICP-AES). The oxidation state of Ni ions in Ni-PiU was studied by X-ray photoelectron spectroscopy (XPS). The obtained spectrum exhibited a Ni 2p_{3/2} binding energy of 856 eV, which represents a Ni²⁺ signal (Figure 2a), based on

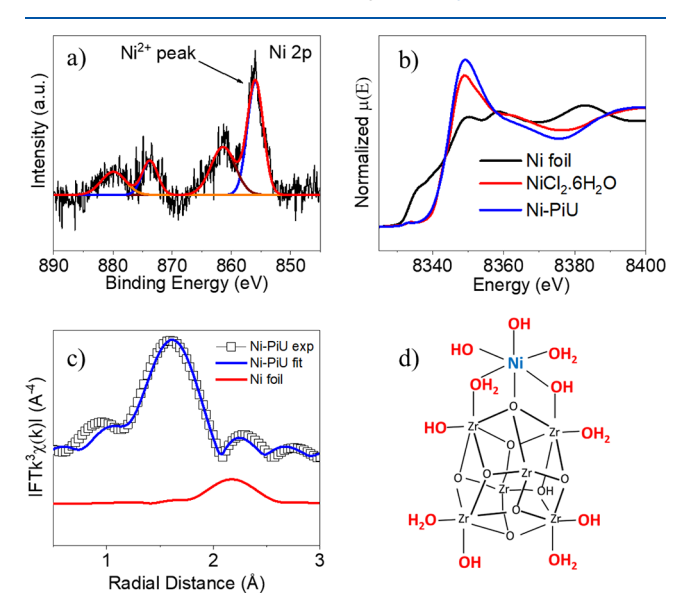


Figure 2. (a) XPS spectra of Ni 2p in Ni-PiU; (b) Ni K-edge XANES spectra of Ni-PiU, NiCl $_2$ ·6H $_2$ O, and Ni foil; (c) EXAFS spectra in the R space of Ni-PiU with its best fitting and Ni foil; (d) structural model used for EXAFS fitting.

reported binding energies of different oxidation states of Ni in the $2p_{3/2}$ core level region. In addition, the observed satellite peak at 861 eV is typical for Ni²⁺ compounds.^{37,38} To gain an in-depth understanding of the electronic and geometric structure of the Ni sites, X-ray absorption spectroscopy (XAS) collected at the Ni K edge was employed. As shown in the X-ray absorption near-edge structure (XANES) spectrum of Ni-PiU (Figure 2b) and its first derivative plot (Figure S6), Ni-PiU absorption edge energy is close to that of NiCl₂·6H₂O, further supporting the existence of Ni²⁺ in Ni-PiU. In addition, a weak pre-edge feature at 8.334 keV

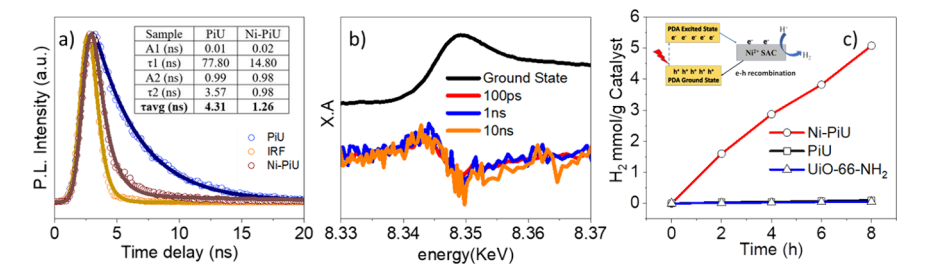


Figure 3. (a) Emission lifetime decay at 530 nm of PiU and Ni-PiU following 415 nm excitation; (b) X-ray transient absorption spectra collected at 100 ps, 1 ns, and 10 ns delay times following 400 nm excitation. The difference spectra were obtained by subtracting the XANES spectra (laser off) from the one with excitation (laser on); (c) photocatalytic H₂ evolution rate of Ni-PiU, PiU, and UiO-66-NH₂. The inset shows the proposed electron transfer in Ni-PiU.

corresponding to 1s-3d dipole-forbidden but quadrupoleallowed transition was observed. This suggests the presence of 3d and 4p orbital hybridization of the Ni central atoms.³⁹ The extended X-ray absorption fine structure (EXAFS) spectrum was used to quantitatively evaluate the local coordination of Ni in Ni-PiU. As shown in Figure 2c, Ni-PiU presented a dominant peak at around 1.56 Å, which corresponds to the Ni-O scattering path. The absence of a Ni-Ni scattering path confirmed the atomic singly dispersed Ni²⁺ in Ni-PiU. EXAFS data fitted with a Ni 4-, 5- (inset of Figure S7a,b), and 6coordinate FEFF model (Figure 2d) using the Artemis X-ray absorption analysis package unravel the local geometry of Ni²⁺. The best-fit results obtained (Table S2) showed a Ni-O bond distance of 2.0735 ± 0.006 Å with each Ni center coordinated to six oxygen atoms, suggesting an octahedral geometry. Combining these results with the observed pre-edge feature at the XANES spectrum, the Ni center in Ni-PiU is mainly dominated by a distorted octahedral geometry.

The charge separation dynamics was examined by using a time-correlated single photon counting (TCSPC) technique and X-ray transient absorption spectroscopy (XTA). As shown in Figure 3a, compared to the emission lifetime decay of PiU, the emission lifetime of Ni-PiU displayed a much faster decay, suggesting the quenching of the PiU excited state in the presence of Ni. To unravel whether electron or hole transfer is responsible for excited state quenching in Ni-PiU, XTA was used to directly probe the change in electron density at the Ni center after photoexcitation at 400 nm. As shown in Figure 3b, a positive peak at 8.345 keV was clearly observed in the transient signal obtained by subtracting the XANES spectrum without photoexcitation from that with photoexcitation, which suggests that the Ni edge shifts to lower energy compared to its ground state. This is a direct support for the reduction of the Ni center after excitation, 40 which unambiguously confirms the electron transfer process from PDA to Ni. The electron transfer time can be estimated from the emission lifetime, according to eq 1.

$$\frac{1}{t_{\text{Ni-PiU}}} = \frac{1}{t_{\text{PiU}}} + \frac{1}{t_{\text{ET}}} \tag{1}$$

where $t_{\rm Ni-PiU}$, $t_{\rm PiU}$, and $t_{\rm ET}$ are the emission lifetimes of Ni-PiU, PiU, and electron transfer time, respectively. According to this equation and the emission lifetime of Ni-PiU (1.26 ns) and PiU (4.31 ns), the ET time was calculated to be 1.78 ns. These results are further supported by the exhibited Ni-PiU higher photocurrent response compared to PiU and UiO-66-NH₂ as shown in Figure S8, indicating that efficient electron transfer in Ni-PiU as a photocurrent response is directly proportional to

charge transfer and carrier mobility.⁴¹ In addition to ET, charge recombination can occur. As indicated by the Ni reduced state in XTA, the reduced Ni shows negligible recovery within 10 ns, suggesting a super-slow charge recombination process. The overall charge separation process is illustrated in the inset of Figure 3c. Following the photoexcitation of PDA, the electrons in excited PDA transfer to the Ni site, resulting in the reduction of the Ni center as evidenced by the quenching of the excited state of PDA (TCSPC) and the reduction of the Ni center (XTA). The reduced Ni center is long-lived (\gg 10 ns), suggesting the great promise to use this system for hydrogen evolution reaction (HER).

Motivated by these photophysical studies in Ni-PiU, we proceeded to evaluate their photocatalytic activity by performing HER under visible light irradiation, where built-in PDA is used as a light-harvesting unit, triethylamine (TEA) as the sacrificial electron donor, and DMF as the reaction medium. These reaction solvents were selected after the systematic screening of the different electron donors and reaction media (Figure S9) to achieve optimum HER activity using Ni-PiU as the catalyst. Control experiments (Figure S10) showed that TEA (electron sacrificial donor), photocatalyst, and light are the key components for the HER, as the absence of any one of these components results in no H2. However, a certain amount of H₂ was produced in the absence of water, suggesting that the sacrificial electron donor TEA has contribution as a proton source under light irradiation.⁴² As shown in Figure S11, variation of the catalyst mass loading in HER shows that the highest catalytic efficiency was observed for the system with 2.5 mg of catalyst loading, after which the efficiency decreases. This might be due to the reduction of photon absorption due to light scattering by the catalyst when the mass loading increases. Under the optimized catalytic conditions with 100 µL of water, 4 mL of DMF, 1 mL of TEA, and 2.5 mg of catalyst mass loading, Ni-PiU exhibited the highest H2 production rate of 0.63 mmol·g⁻¹·h⁻¹ with a turnover number (TON) of 14.15 based on the Ni content (Figure 3c), which is in stark contrast to its counterpart PiU and UiO-66-NH₂, which show H₂ production rates of 0.013 and 0.0066 mmol $g^{-1} \cdot h^{-1}$, respectively. In addition, the recyclability and stability of Ni-PiU were assessed by quenching the reaction after 5 h and separating the catalyst from the reaction medium by centrifugation. The obtained Ni-PiU was then washed with ethanol and redispersed in the catalysis mixture for HER. As highlighted in Figures S12 and S13, the catalytic activity and crystallinity were retained for at least 3 cycles, suggesting the excellent stability and recyclability of Ni-PiU.

4. CONCLUSIONS

In summary, we report the successful synthesis of a hybrid UiO-66-NH₂ MOF system with Ni SACs supported on its Zroxo-cluster metal node and a PDA molecule incorporated to its organic linker to enhance its light-absorbing ability. Using the combination of TCSPC and XTA, we unambiguously confirmed that efficient charge separation occurs in Ni-PiU through electron transfer from PDA to Ni SACs following the excitation of PDA, which is responsible for the significantly enhanced HER performance with respect to its counterparts. This work not only demonstrates the unique capability of MOFs as dual supports for both photosensitizers and SACs to enhance their light absorption and charge separation efficiency but also the ability of time-resolved spectroscopy to examine the fundamental photophysical properties that can provide important insights on rational design of efficient sustainable photocatalytic materials for solar fuel conversion.

ASSOCIATED CONTENT

Supporting Information

The Supporting Information is available free of charge at https://pubs.acs.org/doi/10.1021/acs.jpcc.3c05005.

SEM images, FTIR results, EDX results, ICP-MS results, first derivative XANES graph, EXAFS fitting results, photocurrent response results, H_2 photocatalytic optimization and control reactions, and photocatalyst recyclability and stability experiments (PDF)

AUTHOR INFORMATION

Corresponding Author

Jier Huang — Department of Chemistry, Marquette University, Milwaukee, Wisconsin 53201, United States; Department of Chemistry and Schiller Institute for Integrated Science and Society, Boston College, Chestnut Hill, Massachusetts 02467, United States; orcid.org/0000-0002-2885-5786; Email: jier.huang@bc.edu

Authors

Humphrey Chiromo – Department of Chemistry, Marquette University, Milwaukee, Wisconsin 53201, United States

James Nyakuchena – Department of Chemistry, Marquette University, Milwaukee, Wisconsin 53201, United States

Daniel Streater – Department of Chemistry, Marquette University, Milwaukee, Wisconsin 53201, United States

Qiushi Ma – Department of Chemistry and Schiller Institute for Integrated Science and Society, Boston College, Chestnut Hill, Massachusetts 02467, United States

Christopher Turchiano – Department of Chemistry and Biochemistry, San Diego State University, San Diego, California 92182, United States; orcid.org/0000-0003-3173-3795

Xiaoyi Zhang — X-ray Science Division, Argonne National Laboratory, Argonne, Illinois 60349, United States;
orcid.org/0000-0001-9732-1449

Jing Gu — Department of Chemistry and Biochemistry, San Diego State University, San Diego, California 92182, United States; ⊚ orcid.org/0000-0002-5506-0049

Complete contact information is available at: https://pubs.acs.org/10.1021/acs.jpcc.3c05005

Notes

The authors declare no competing financial interest.

ACKNOWLEDGMENTS

This work was supported by the National Science Foundation under award number CSDM-B-2321203. The use of the Advanced Photon Source in Argonne National Laboratory was supported by the U.S. Department of Energy, Office of Science, Office of Basic Energy Sciences, under award no. DE-AC02-06CH11357.

REFERENCES

- (1) Yan, J.; Kong, L.; Ji, Y.; White, J.; Li, Y.; Zhang, J.; An, P.; Liu, S.; Lee, S.-T.; Ma, T. Single atom tungsten doped ultrathin α -Ni (OH) 2 for enhanced electrocatalytic water oxidation. *Nat. Commun.* **2019**, *10* (1), 1–10.
- (2) Jiao, L.; Jiang, H.-L. Metal-organic-framework-based single-atom catalysts for energy applications. *Chem* **2019**, *5* (4), 786–804.
- (3) Qiao, B.; Wang, A.; Yang, X.; Allard, L. F.; Jiang, Z.; Cui, Y.; Liu, J.; Li, J.; Zhang, T. Single-atom catalysis of CO oxidation using Pt1/FeOx. *Nat. Chem.* **2011**, *3* (8), 634–641.
- (4) Abbet, S.; Sanchez, A.; Heiz, U.; Schneider, W.-D.; Ferrari, A. M.; Pacchioni, G.; Rösch, N. Acetylene cyclotrimerization on supported size-selected Pd n clusters ($1 \le n \le 30$): One atom is enough! *J. Am. Chem. Soc.* **2000**, *122* (14), 3453–3457.
- (5) Hackett, S. F.; Brydson, R. M.; Gass, M. H.; Harvey, I.; Newman, A. D.; Wilson, K.; Lee, A. F. High-activity, single-site mesoporous Pd/Al2O3 catalysts for selective aerobic oxidation of allylic alcohols. *Angew. Chem.* **2007**, *119* (45), 8747–8750.
- (6) Fu, Q.; Saltsburg, H.; Flytzani-Stephanopoulos, M. Active nonmetallic Au and Pt species on ceria-based water-gas shift catalysts. *Science* **2003**, *301* (5635), 935–938.
- (7) Yang, X.-F.; Wang, A.; Qiao, B.; Li, J.; Liu, J.; Zhang, T. Singleatom catalysts: a new frontier in heterogeneous catalysis. *Acc. Chem. Res.* **2013**, *46* (8), 1740–1748.
- (8) Lin, Y.; Liu, P.; Velasco, E.; Yao, G.; Tian, Z.; Zhang, L.; Chen, L. Fabricating single-atom catalysts from chelating metal in open frameworks. *Adv. Mater.* **2019**, *31* (18), 1808193.
- (9) Zhang, H.; Liu, G.; Shi, L.; Ye, J. Single-atom catalysts: emerging multifunctional materials in heterogeneous catalysis. *Adv. Energy Mater.* **2018**, 8 (1), 1701343.
- (10) Qin, R.; Liu, P.; Fu, G.; Zheng, N. Strategies for stabilizing atomically dispersed metal catalysts. *Small Methods* **2018**, 2 (1), 1700286.
- (11) Wang, A.; Li, J.; Zhang, T. Heterogeneous single-atom catalysis. *Nat. Rev. Chem.* **2018**, 2 (6), 65–81.
- (12) James, T. E.; Hemmingson, S. L.; Campbell, C. T. Energy of supported metal catalysts: from single atoms to large metal nanoparticles. *ACS Catal.* **2015**, *5* (10), 5673–5678.
- (13) Zhang, B.; Fan, T.; Xie, N.; Nie, G.; Zhang, H. Versatile Applications of Metal Single-Atom@ 2D Material Nanoplatforms. Adv. Sci. 2019, 6 (21), 1901787.
- (14) Liu, H.; Cheng, M.; Liu, Y.; Wang, J.; Zhang, G.; Li, L.; Du, L.; Wang, G.; Yang, S.; Wang, X. Single atoms meet metal—organic frameworks: collaborative efforts for efficient photocatalysis. *Energy Environ. Sci.* **2022**, *15* (9), 3722–3749.
- (15) Li, B.; Wen, H. M.; Cui, Y.; Zhou, W.; Qian, G.; Chen, B. Emerging multifunctional metal—organic framework materials. *Adv. Mater.* **2016**, 28 (40), 8819–8860.
- (16) Jiao, L.; Zhang, R.; Wan, G.; Yang, W.; Wan, X.; Zhou, H.; Shui, J.; Yu, S.-H.; Jiang, H.-L. Nanocasting SiO2 into metal—organic frameworks imparts dual protection to high-loading Fe single-atom electrocatalysts. *Nat. Commun.* **2020**, *11* (1), 1–7.
- (17) Drake, T.; Ji, P.; Lin, W. Site isolation in metal-organic frameworks enables novel transition metal catalysis. *Acc. Chem. Res.* **2018**, *51* (9), 2129–2138.
- (18) Huang, H.; Shen, K.; Chen, F.; Li, Y. Metal-organic frameworks as a good platform for the fabrication of single-atom catalysts. *ACS Catal.* **2020**, *10* (12), 6579–6586.
- (19) Qu, W.; Chen, C.; Tang, Z.; Wen, H.; Hu, L.; Xia, D.; Tian, S.; Zhao, H.; He, C.; Shu, D. Progress in metal-organic-framework-based

- single-atom catalysts for environmental remediation. *Coord. Chem. Rev.* 2023, 474, 214855.
- (20) Szilágyi, P. Á.; Rogers, D. M.; Zaiser, I.; Callini, E.; Turner, S.; Borgschulte, A.; Züttel, A.; Geerlings, H.; Hirscher, M.; Dam, B. Functionalised metal—organic frameworks: a novel approach to stabilising single metal atoms. *J. Mater. Chem. A* **2017**, *5* (30), 15559–15566.
- (21) Neumann, M.; Füldner, S.; König, B.; Zeitler, K. Metal-free, cooperative asymmetric organophotoredox catalysis with visible light. *Angew. Chem., Int. Ed.* **2011**, *50* (4), 951–954.
- (22) Li, L.; Wang, X.; Liu, T.; Ye, J. Titanium-Based MOF Materials: From Crystal Engineering to Photocatalysis. *Small Methods* **2020**, *4* (12), 2000486.
- (23) He, J.; Wang, J.; Chen, Y.; Zhang, J.; Duan, D.; Wang, Y.; Yan, Z. A dye-sensitized Pt@UiO-66(Zr) metal—organic framework for visible-light photocatalytic hydrogen production. *Chem. Commun.* **2014**, *50* (53), 7063–7066.
- (24) Fu, Y.; Sun, D.; Chen, Y.; Huang, R.; Ding, Z.; Fu, X.; Li, Z. An amine-functionalized titanium metal—organic framework photocatalyst with visible-light-induced activity for CO2 reduction. *Angew. Chem., Int. Ed.* **2012**, *51* (14), 3364–3367.
- (25) Guo, D.; Wen, R.; Liu, M.; Guo, H.; Chen, J.; Weng, W. Facile fabrication of g-C3N4/MIL-53(Al) composite with enhanced photocatalytic activities under visible-light irradiation. *Appl. Organomet. Chem.* **2015**, 29 (10), 690–697.
- (26) Elcheikh Mahmoud, M.; Audi, H.; Assoud, A.; Ghaddar, T. H.; Hmadeh, M. Metal—Organic Framework photocatalyst Incorporating Bis(4'-(4-carboxyphenyl)-terpyridine)ruthenium(II) for Visible-Light-Driven Carbon Dioxide Reduction. *J. Am. Chem. Soc.* **2019**, 141 (17), 7115–7121.
- (27) Hendrickx, K.; Joos, J. J.; De Vos, A.; Poelman, D.; Smet, P. F.; Van Speybroeck, V.; Van Der Voort, P.; Lejaeghere, K. Exploring lanthanide doping in UiO-66: a combined experimental and computational study of the electronic structure. *Inorg. Chem.* **2018**, *57* (9), 5463–5474.
- (28) Yu, H.; Joo, P.; Lee, D.; Kim, B. S.; Oh, J. H. Photoinduced Charge-Carrier Dynamics of Phototransistors Based on Perylene Diimide/Reduced Graphene Oxide Core/Shell p—n Junction Nanowires. *Adv. Opt. Mater.* **2015**, 3 (2), 241–247.
- (29) Schaate, A.; Roy, P.; Godt, A.; Lippke, J.; Waltz, F.; Wiebcke, M.; Behrens, P. Modulated synthesis of Zr-based metal—organic frameworks: from nano to single crystals. *Chem. Eur. J.* **2011**, *17* (24), 6643–6651.
- (30) Wang, H.; Wang, H.; Wang, Z.; Tang, L.; Zeng, G.; Xu, P.; Chen, M.; Xiong, T.; Zhou, C.; Li, X.; Huang, D.; Zhu, Y.; Wang, Z.; Tang, J. Covalent organic framework photocatalysts: structures and applications. *Chem. Soc. Rev.* **2020**, *49* (12), 4135–4165.
- (31) Nyakuchena, J.; Ostresh, S.; Streater, D.; Pattengale, B.; Neu, J.; Fiankor, C.; Hu, W.; Kinigstein, E. D.; Zhang, J.; Zhang, X.; Schmuttenmaer, C. A.; Huang, J. Direct evidence of photoinduced charge transport mechanism in 2D conductive metal organic frameworks. J. Am. Chem. Soc. 2020, 142 (50), 21050–21058.
- (32) Luu, C. L.; Nguyen, T. T. V.; Nguyen, T.; Hoang, T. C. Synthesis, characterization and adsorption ability of UiO-66-NH2. *Adv. Nat. Sci.: Nanosci. Nanotechnol.* **2015**, *6* (2), No. 025004.
- (33) Wang, J.; Liu, X.; Li, C.; Yuan, M.; Zhang, B.; Zhu, J.; Ma, Y. Fabrication of perylene imide-modified NH2-UiO-66 for enhanced visible-light photocatalytic degradation of tetracycline. *J. Photochem. Photobiol.*, A 2020, 401, 112795.
- (34) Tahir, M.; Muddusir; Khan, D. N.; Gul, S.; Wahab, F.; Said, S. M. Photovoltaic effect on the microelectronic properties of perylene/p-Si heterojunction devices. *J. Mater. Sci.: Mater. Electron.* **2019**, *30*, 19463–19470.
- (35) Sengupta, S.; Dubey, R. K.; Hoek, R. W. M.; van Eeden, S. P. P.; Gunbaş, D. D.; Grozema, F. C.; Sudhölter, E. J. R.; Jager, W. F. Synthesis of regioisomerically pure 1, 7-dibromoperylene-3,4,9,10-tetracarboxylic acid derivatives. *J. Org. Chem.* **2014**, 79 (14), 6655–6662.

- (36) Tian, H.; Liu, P.-H.; Zhu, W.; Gao, E.; Wu, D.-J.; Cai, S. Synthesis of novel multi-chromophoric soluble perylene derivatives and their photosensitizing properties with wide spectral response for SnO2 nanoporous electrode. *J. Mater. Chem.* **2000**, *10* (12), 2708–2715
- (37) Al-Kuhaili, M. F.; Ahmad, S. H. A.; Durrani, S. M. A.; Faiz, M. M.; Ul-Hamid, A. Application of nickel oxide thin films in NiO/Ag multilayer energy-efficient coatings. *Mater. Sci. Semicond. Process.* **2015**, *39*, 84–89.
- (38) Niklasson, G. A.; Granqvist, C. G. Electrochromics for smart windows: thin films of tungsten oxide and nickel oxide, and devices based on these. *J. Mater. Chem.* **2007**, *17* (2), 127–156.
- (39) Yamamoto, T. Assignment of pre-edge peaks in K-edge x-ray absorption spectra of 3d transition metal compounds: Electric dipole or quadrupole? *X-Ray Spectrom.: Int. J.* **2008**, 37 (6), 572–584.
- (40) Yang, S.; Fan, D.; Hu, W.; Pattengale, B.; Liu, C.; Zhang, X.; Huang, J. Elucidating charge separation dynamics in a hybrid metalorganic framework photocatalyst for light-driven H2 evolution. *J. Phys. Chem. C* **2018**, *122* (6), 3305–3311.
- (41) Liu, Y.; Xie, C.; Li, J.; Zou, T.; Zeng, D. New insights into the relationship between photocatalytic activity and photocurrent of TiO2/WO3 nanocomposite. *Appl. Catal. A* **2012**, *433-434*, 81–87.
- (42) Yang, R.; Song, K.; He, J.; Fan, Y.; Zhu, R. Photocatalytic hydrogen production by RGO/ZnIn2S4 under visible light with simultaneous organic amine degradation. *ACS omega* **2019**, *4* (6), 11135–11140.